Biomolecular Characterization and Protein Sequences of the Campanian Hadrosaur B. canadensis

Mary H. Schweitzer, *et al.*

Science **324**, 626 (2009);
DOI: 10.1126/science.1165069

Biomolecular Characterization and Protein Sequences of the Campanian Hadrosaur *B. canadensis*

Mary H. Schweitzer,[1,2]* Wenxia Zheng,[1] Chris L. Organ,[3] Recep Avci,[4] Zhiyong Suo,[4] Lisa M. Freimark,[5] Valerie S. Lebleu,[6,7] Michael B. Duncan,[6,7] Matthew G. Vander Heiden,[8] John M. Neveu,[9] William S. Lane,[9] John S. Cottrell,[10] John R. Horner,[11] Lewis C. Cantley,[5,12] Raghu Kalluri,[6,7,13] John M. Asara[5,14]*

Molecular preservation in non-avian dinosaurs is controversial. We present multiple lines of evidence that endogenous proteinaceous material is preserved in bone fragments and soft tissues from an 80-million-year-old Campanian hadrosaur, *Brachylophosaurus canadensis* [Museum of the Rockies (MOR) 2598]. Microstructural and immunological data are consistent with preservation of multiple bone matrix and vessel proteins, and phylogenetic analyses of *Brachylophosaurus* collagen sequenced by mass spectrometry robustly support the bird-dinosaur clade, consistent with an endogenous source for these collagen peptides. These data complement earlier results from *Tyrannosaurus rex* (MOR 1125) and confirm that molecular preservation in Cretaceous dinosaurs is not a unique event.

Soft tissues and cell-like structures observed in a variety of vertebrate fossils (*1*, *2*) raise the question of whether, and to what extent, original molecular components remain associated with these structures and the bones containing them. A suite of experiments supported the presence of original collagen molecules in the bony matrix of *Tyrannosaurus rex* [Museum of the Rockies (MOR) 1125] (*3*), and phylogenetic analysis of tryptic fragments sequenced by mass spectrometry (*4*, *5*) placed *T. rex* within Archosauria, closer to birds than other vertebrate taxa in the sampled database (*6*, but see also *7*–*10*).

Deep burial in sandstone seems to favor exceptional preservation (*2*). We recovered a single femur from an articulated hind limb of *Brachylophosaurus canadensis* (MOR 2598). The pes elements, tibia, and fibula were collected in 2006; the femur was untouched and protected under ~7 m of Judith River Fomation sandstones, Eastern Montana, USA, until recovery in 2007. The femur was not exposed in the field but jacketed with ~10 to 12 cm of sediments to maintain equilibrium. Immediately after opening the jacket, bone and sediment samples were collected with sterile instruments, wrapped in layers of foil, and placed in sealed jars with desiccation crystals until laboratory analyses were performed. Bone and/or processed samples were dispersed to multiple institutions for independent analyses. Some bone fragments were subjected to chemical extraction (*3*, *10*), and others were demineralized, showing marked preservation of microstructures resembling soft, transparent vessels, cells, and fibrous matrix in this pristine bone (Fig. 1 and fig. S1) (*10*).

Under field-emission scanning electron microscopy (FESEM) (*10*), demineralized bone matrix was fibrous, with fibers arranged either in distinct layers at ~30° (Fig. 1A) that retain the original plywoodlike orientation of collagen fibers in bone (*11*, *12*) or arranged in parallel (Fig. 1B). Microstructures with filipodial extensions and internal contents, consistent in size and morphology to vertebrate osteocytes (*13*, *14*), were visible at matrix layer boundaries (Fig. 1A, arrows). The matrix was virtually indistinguishable from recent demineralized ostrich bone (Fig. 1C) imaged under the same parameters. In transmitted light, demineralized matrix appeared white and fibrous (Fig. 1D) and autofluoresced when illuminated with a mercury lamp, similar to extant bone collagen (*15*).

Transparent, flexible vessels were observed; some contained spherical microstructures (Fig. 1E), whereas others contained an amorphous red substance (Fig. 1F) that is superficially similar to degraded blood products in vessels recovered from extant bone (Fig. 1G) (*2*). *B. canadensis* vessels were hollow (Fig. 1H), with walls of uniform thickness, and possessed a surface texture that differed from exterior to luminal surfaces, features not consistent with the relatively amorphous texture of biofilm (*7*). Vessel surface texture differed substantially from the fibrous matrix but was similar to that seen in extant ostrich vessels (Fig. 1I) (*1*) after demineralization and collagenase digestion. Osteocytes were closely associated with vessels in both extant and *B. canadensis* samples (Fig. 1, H and I, arrows). The variation in texture, microstructure, and color of dinosaur material is consistent with extant tissues and not plausibly explained by biofilm (*7*).

Ovoid red "cells" with long filipodia, similar in morphology to extant osteocytes, were embedded in or associated with white matrix (Fig. 1J and fig. S1) or vessels (Fig. 1H). In some cases, these were attached by their filipodia to adjacent cells (Fig. 1J, inset), forming an interconnecting network as in extant bone. The cells contain internal microstructures suggestive of nuclei. Red filipodia extend from cell bodies into the white fibrous matrix (Fig. 1J and fig. S1), reflecting original chemical differences at submicron levels between cells and matrix and inconsistent with recent microbial invasion (*7*). Under FESEM (*10*), *B. canadensis* osteocytes and filipodia (Fig. 1K) are similar in morphology, surface texture, and size to extant ostrich osteocytes isolated from bone digests (Fig. 1L) (*1*, *2*, *13*, *14*).

MOR 2598 bone fragments were chemically extracted (*2*, *10*) for use in multiple analyses. Electrophoretic separation revealed a smear of silver-stainable material, not present in either buffer controls or surrounding sediment extracted in tandem with the bone. A dark-staining high–molecular weight band was consistently seen in guanidine extracts, whereas a low–molecular weight smear was visible in trichloroacetic acid extractions (fig. S2) (*10*).

Both chemical extracts and demineralized dinosaur tissues showed binding of antibodies raised against collagen and other extant proteins. Enzyme-linked immunosorbent assays (fig. S3A) and immunoblots (figs. S3B and S9) of bone extracts showed positive reactivity to antibodies raised against avian collagen I and/or osteocalcin; controls of extraction buffers alone or coextracted sediments were nonreactive (figs. S3A and S9). Results were repeated in two separate laboratories (labs of R.K. and L.C.C.) on separate extractions of MOR 2598 bone fragments.

In situ immunohistochemical analyses conducted on demineralized dinosaur extracellular matrix showed positive reactivity to polyclonal antibodies raised against avian collagen I (Fig. 2A), osteocalcin (Fig. 2D), and ostrich whole bone extracts (fig. S4) (*10*), but monoclonal antibodies raised against a specific osteocalcin epitope (fig. S5) showed no binding. This may indicate that the single epitope targeted by the monoclonal antibody was either not preserved or not present originally in *B. canadensis* protein. Negative controls of secondary antibody only (no primary added) showed no binding (fig. S5), and specificity controls of inhibition (blocking antibody binding sites by first incubating with excess collagen, see Fig. 2B) and tissue digestion with collagenase before antibody exposure (Fig. 2C) resulted in the reduction of binding. Antibodies to ostrich whole bone extracts (fig. S4) bound dinosaur tissues slightly stronger than commercial

[1]North Carolina State University, Raleigh, NC 27695, USA. [2]North Carolina Museum of Natural Sciences, Raleigh, NC 27601, USA. [3]Department of Organismic and Evolutionary Biology, Harvard University, Cambridge, MA 02138, USA. [4]Imaging and Chemical Analysis Laboratory, Montana State University, Bozeman, MT 59717, USA. [5]Division of Signal Transduction, Beth Israel Deaconess Medical Center, Boston, MA 02115, USA. [6]Division of Matrix Biology, Beth Israel Deaconess Medical Center, Boston, MA 02115, USA. [7]Department of Medicine, Harvard Medical School, Boston, MA 02115, USA. [8]Dana Farber Cancer Institute, Boston, MA 02115, USA. [9]Faculty of Arts and Sciences Center for Systems Biology, Harvard Univeristy, Cambridge, MA 02138, USA. [10]Matrix Science Ltd., 64 Baker Street, London, W1U 7GB, UK. [11]Museum of the Rockies, Bozeman, MT 59717, USA. [12]Department of Systems Biology, Harvard Medical School, Boston, MA 02115, USA. [13]Department of Biological Chemistry and Molecular Pharmacology and Harvard-MIT Division of Health Sciences and Technology, Harvard University, Cambridge, MA 02139, USA. [14]Department of Pathology, Harvard Medical School, Boston, MA 02115, USA.

*To whom correspondence should be addressed. E-mail: schweitzer@ncsu.edu (M.H.S.); jasara@bidmc.harvard.edu (J.M.A.)

chicken collagen antibodies (Fig. 2A), possibly indicating more shared epitopes between *B. canadensis* and ostrich bone proteins than this dinosaur and chicken. These results support the hypothesis that original epitopes of bone proteins are preserved in these 80-million-year-old dinosaur skeletal elements.

Because elastin, laminin, and hemoglobin are commonly associated with blood vessels in tetrapods, we used antibodies raised against these proteins to test for epitopes preserved in *B. canadensis* vessels. Elastin is a highly conserved, vertebrate-specific molecule generally resistant to degradation (*16*), and antibodies to this protein bound dinosaur vessels above background levels in all cases, both

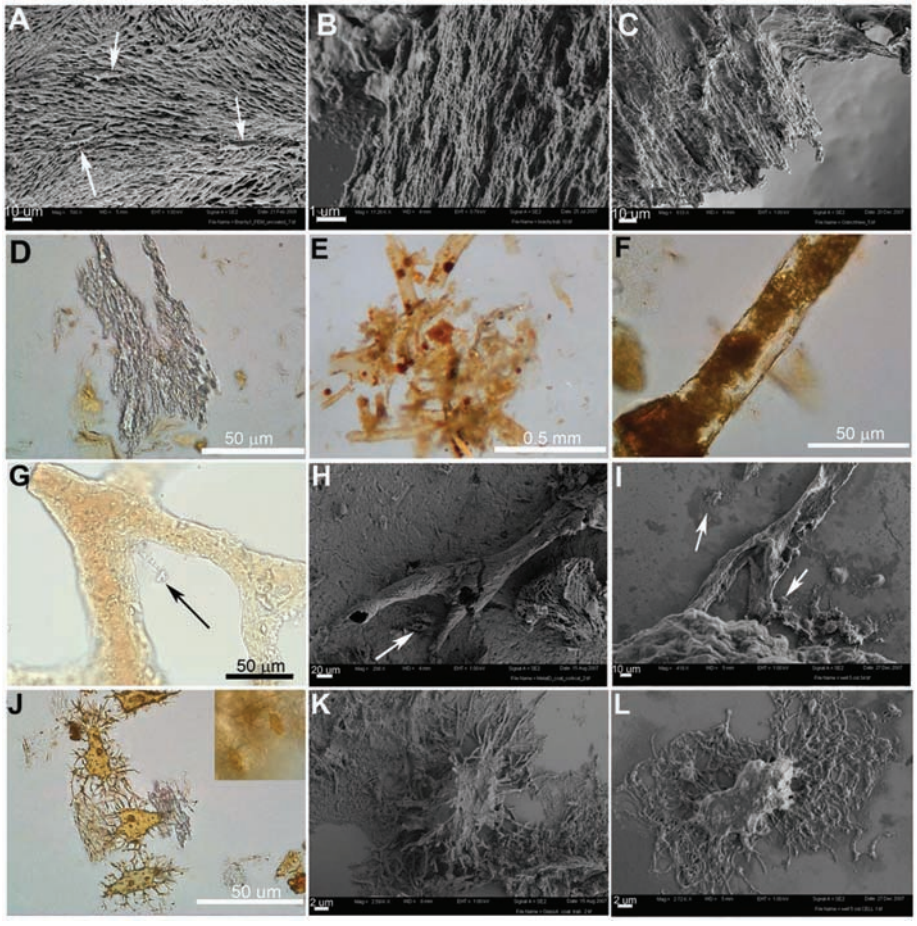

Fig. 1. FESEM and transmitted light micrographs of demineralized *B. canadensis* (MOR 2598) bone matrix, vessels, and cells, compared with extant ostrich components imaged under similar conditions. (**A**) Low-magnification of FESEM demineralized MOR 2598 shows fibers in a plywood-like array characteristic of bone. Arrows indicate osteocytes in lacunae within fibers. (**B**) Demineralized matrix showing detail of fibers. (**C**) Demineralized ostrich bone matrix imaged under the same parameter as in (B). (**D**) Demineralized bone matrix from MOR 5928 is white under transmitted light. (**E**) MOR 2598 vessels and matrix after EDTA demineralization show rounded red inclusions (*10*). (**F**) Higher magnification of isolated MOR 5923 vessel, showing amorphous red intravascular contents. (**G**) Ostrich vessel with amorphous contents and associated osteocyte (arrow). (**H**) FESEM shows hollow *B. canadensis* vessels, often associated with osteocytes (arrow). (**I**) FESEM image of collapsed ostrich vessel and associated matrix with osteocytes (arrows). (**J**) Osteocytes attached by interconnected filipodia, with filipodia embedded in fibrous matrix. (**K**) FESEM of single *B. canadensis* osteocyte with long filipodia. (**L**) Single ostrich osteocyte isolated from demineralized, digested bone.

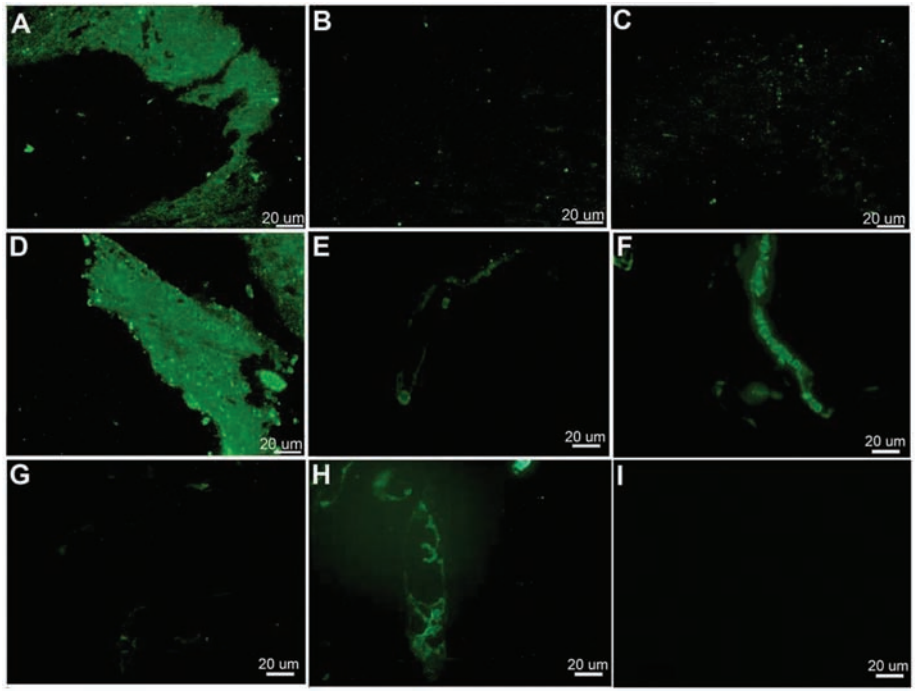

Fig. 2. In situ immunohistochemistry of demineralized *B. canadensis* bone matrix and vessels. (**A**) Incubated with antibodies against avian collagen I . (**B**) Anti-collagen antibodies inhibited with avian collagen, then incubated with tissues as in (A). (**C**) Demineralized bone matrix digested with collagenase, then incubated with anti-collagen antibodies as in (A). (**D**) *B. canadensis* demineralized bone matrix incubated with anti-osteocalcin polyclonal antibodies (*10*). (**E**) *B. canadensis* vessels incubated with polyclonal antibodies against laminin (*10*) show weak binding above background levels. (**F**) Vessels incubated with antibodies against elastin proteins. (**G**) Vessels digested with elastase, then incubated with elastin antibodies as in (F). (**H**) *B. canadensis* vessels incubated with polyclonal antibodies against ostrich hemoglobin. (**I**) Ostrich hemoglobin antibodies incubated with excess hemoglobin to inhibit binding, then incubated with dinosaur vessels as in (H). Panels (A) to (D) were taken at 79-ms integration, 63× objective; (E) to (I) were taken at 120-ms integration, 63× objective, magnification as shown.

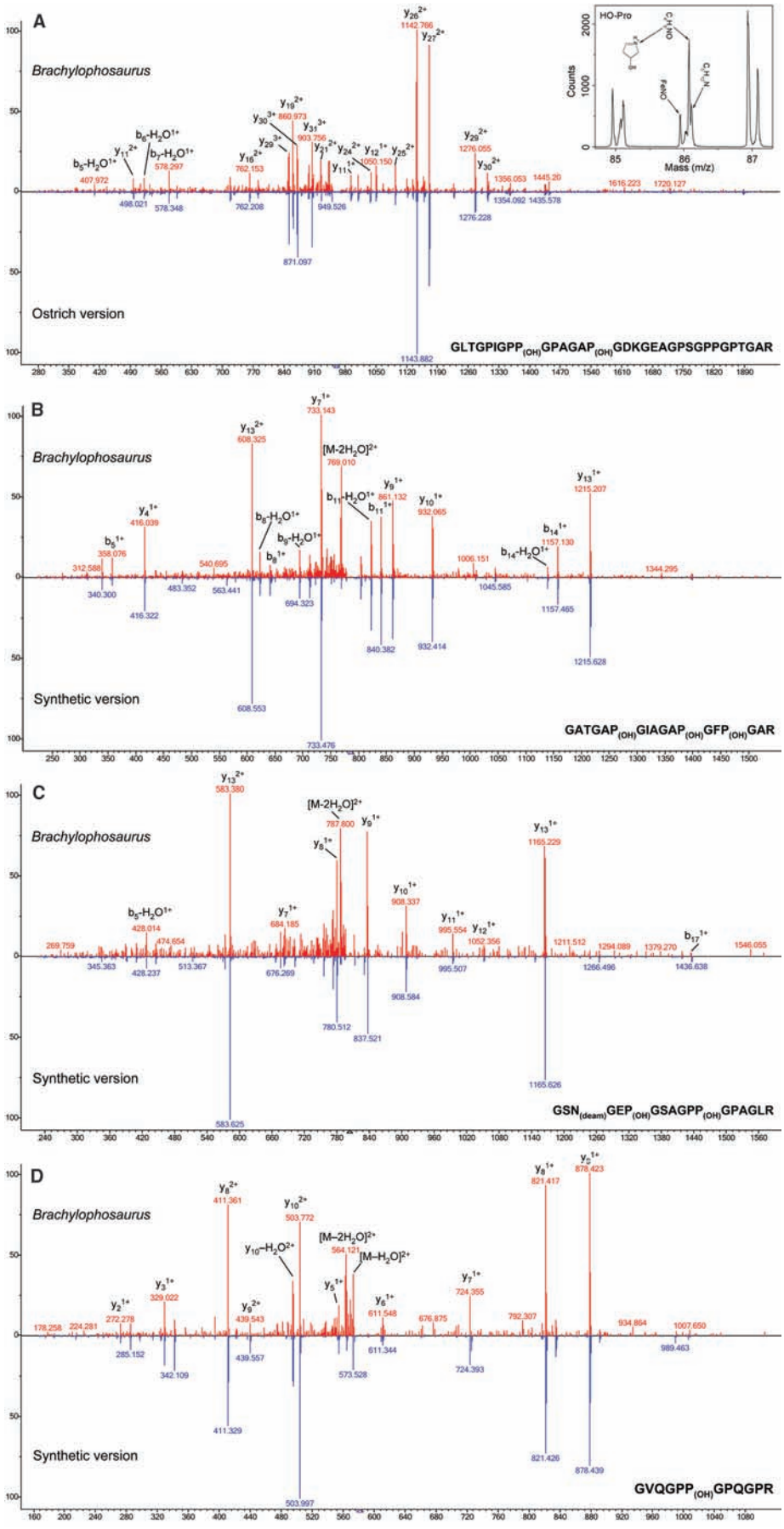

Fig. 3. Mass spectrometry analyses of *B. canadensis* tissues and extracts. (Inset to A) Collagen-specific Pro-OH functional group positively identified by TOF-SIMS in situ analysis of demineralized *B. canadensis* tissues by a preparation method distinct from tandem mass spectrometry analyses [see text and (*10*)]. (**A** to **D**) Product ion spectra recorded during tandem mass spectrometry (LC/MS/MS) analyses with CID of chemical extracts of bone. The four collagen peptides scoring lowest on Mascot search engine scores (but top-ranked versus the Swiss-Prot database) acquired from the LTQ-Orbitrap XL mass spectrometry were validated with high-confidence versions of the same sequences with a computational spectral comparison tool. (A) *B. canadensis* collagen a1(I) [M+3H]3+ peptide ion GLTGPIGPP(OH)GPAGAP (OH)GDKGEAGPSGPPGPTGAR using the MS Search 2.0 spectral comparison algorithm shows excellent alignment of fragment ion *m/z* values and relative intensities and was ranked first to a previously acquired high-confidence ostrich version of the same sequence [reverse match factor (RMF = 779)] in a database of >200,000 spectra. (B) Collagen a1(I) [M+2H]2+ peptide ion GATGAP(OH)GIAGAP(OH)GFP(OH)GAR was a top match to the synthetic peptide version of the same sequence (RMF = 494). (C) The collagen a2(I) [M+2H]2+ peptide ion GSN(deam)GEP(OH)GSAGPP(OH)GPAGLR versus a synthetically derived version (RMF = 482), and (D) the collagen a1(I) [M+2H]2+ peptide ion GVQGPP(OH)GPQGPR validated with a synthetic peptide (RMF = 562). (B, C, and D) Significant fragment ions attributed to water losses from the precursor ion are present in the spectra from *Brachylophosaurus* but are less apparent in synthetic or ostrich comparisons. The four other highest-scoring statistically significant MS/MS spectra are shown in fig. S9 in the SOM.

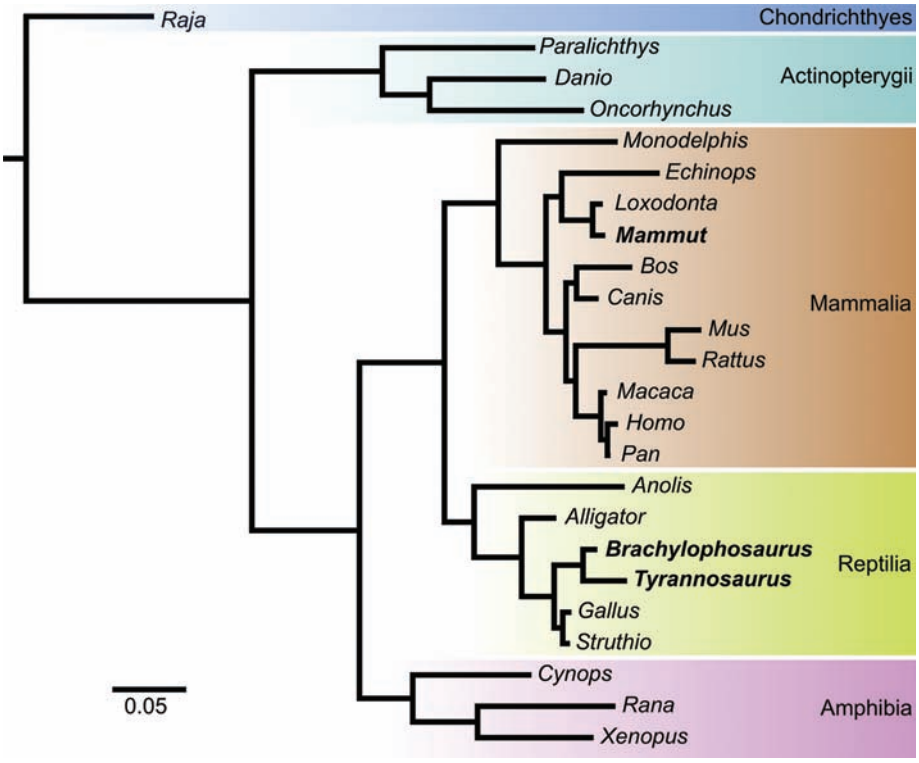

Fig. 4. Consensus of the posterior distribution of phylogenetic trees including *M. americanum* (Mastodon, MOR 605) and the extinct dinosaurs *B. canadensis* (MOR 2598) and *T. rex* (MOR 1125, in bold). Colored backgrounds designate monophyletic groups. All nodes have 100% posterior probability (PP) support except the *Gallus/Struthio* group, which has 36% PP support. Branch lengths are reported as the mean of the expected number of changes per site.

in immunohistochemistry (Fig. 2F) and immunoblot (fig. S6A). Antibodies to both laminin and elastin proteins showed specific binding, though they differed in binding strength in both assays. Three relatively high–molecular weight bands can be seen within a smear of stained material in immunoblot (fig. S6A, thin arrows), whereas two faint bands indicating laminin antibody binding were observed at different molecular weights when compared with elastin-reactive bands (fig. S6A, short arrows). Vessel extracts did not show binding to antibodies raised against ostrich hemoglobin, but hemoglobin antibodies bound specifically in in situ tests (Fig. 2H). A second set of experiments, conducted in a separate lab (by R.K.), confirm these results (fig. S6B). Laminin antibodies known to react to avian and reptilian proteins (*10*) demonstrate specific binding to *B. canadensis* extracts. Controls for spurious antibody binding were negative.

Attenuated total reflection infrared spectroscopy demonstrated clear amide I and amide II bands (fig. S7) in lyophilized vessels and surrounding demineralized matrix. This method cannot be used to identify which proteins are present or the source/endogeneity of these proteins, only characteristic bond vibration patterns. However, the data are consistent with other in situ data supporting the presence of proteinaceous material in *B. canadensis* tissues.

Posttranslational hydroxylation of proline is an identifying feature of collagen, and microbes cannot produce this modification (*17*, *18*). Whole vessels and matrix from demineralized *B. canadensis* bone

Table 1. Collagen α1(I) and α2(I) sequences acquired by ion trap and Orbitrap mass spectrometry for *B. canadensis*. *m/z* values of the peptide ion, molecular weight, mass spectrometer used, database search engine scores, expectation values, sequence validation method, and sequence identity based on BLAST searches versus the all-species NCBInr protein database and internally acquired ostrich and alligator sequences are shown. The interpretation of the sequence GLPGESGAVGPAGPP$_{(OH)}$GSR was aided by the high mass accuracy of the Orbitrap, because hydroxyproline is more accurate than isoleucine/leucine at position 15 by 0.0364 daltons.

m/z (obsd)	Mr (calc)	Mass error	Instrument	rank	Mascot score	Mascot expectation value	Sequest Xcorr	Validation	Peptide sequence	Protein	BLAST sequence identity
960.487	2878.421	0.0047*	Orbitrap	1	40.0	0.59	4.53	Search stats; ostrich peptide	GLTGPIGPP(OH)GPAGAP(OH) GDKGEAGPSGPPGPTGAR	Collagen α1(1)	Ostrich and mammals
730.740	1458.685	0.7793	Ion trap	1	73.7	0.00027	3.99	Search stats	GSAGPP(OH)GATGFP(OH) GAAGR	Collagen α1(1)	*T. rex*, chicken, and mammals
786.901	1571.769	0.0180*	Orbitrap	1	37.2	0.84	3.13	Search stats; synthetic peptide	GATGAP(OH)GIAGAP(OH) GFP(OH)GAR	Collagen α1(1)	*T. rex*, chicken, alligator, and amphibia
766.877	1531.738	0.0005	Orbitrap	1	52.7	0.023	2.70	Search stats	GETGPAGPAGPP(OH)GPAGAR	Collagen α1(1)	Chicken
582.160	1161.589	0.7164	Ion trap	1	65.8	0.0015	2.48	Search stats; synthetic peptide	GVQGPP(OH)GPQGPR	Collagen α1(1)	*T. rex*, chicken, alligator, and opossum
653.824	1305.631	0.0013	Orbitrap	1	56.9	0.012	2.63	Search stats	GPSGPQGPSGAP(OH)GPK	Collagen α1(1)	Chicken, alligator, rat, and opossum
805.875	1609.734	0.0012	Orbitrap	1	40.5	0.54	2.32	Search stats; synthetic peptide	GSN(deam)GEP(OH)GSAGPP (OH)GPAGLR	Collagen α2(1)	Chicken and alligator
789.898	1577.782	0.0005	Orbitrap	1	54.3	0.023	3.97	Search stats	GLPGESGAVGPAGPP(OH)GSR	Collagen α2(1)	*T. rex*

*For two sequences [GLTGPIGPP$_{(OH)}$ GPAGAP$_{(OH)}$ GDKGEAGPSGPPGPTGAR and GATGAP$_{(OH)}$GIAGAP$_{(OH)}$GFP$_{(OH)}$GAR] acquired with the Orbitrap, MS/MS was triggered on the *m/z* ratio representing the ^{13}C stable isotope containing ion rather than the monoisotopic version.

were subjected to in situ time-of-flight–secondary ion mass spectrometry (ToF-SIMS) with imaging capability (*10*) in a separate laboratory (the lab of R.A.). Focused Ga^+ and Au^+ ions generated molecular fragments from tissues that were detected with sufficient high mass resolution ($m/\Delta m \sim 4000$) to uniquely identify hydroxylated proline (Pro-OH), as well as Lys, Pro, Lys-OH, Ala, Gly, and Leu from demineralized dinosaur tissues (fig. S8). A number of organic fragments containing nitrogen were also detected, including unusual complexes between C, N, and Fe (Fig. 3A, inset, and fig. S8), suggesting alteration and modification to preserved organics, more consistent with an ancient source than recent contamination.

We used mass spectrometry (performed by J.M.A.) to analyze whole bone extracts of *B. canadensis* (MOR 2598) that were fibrous and lighter in color than those from *T. rex* (MOR 1125) (*4*, *5*). Bone extracts (*10*) were proteolyzed with trypsin, purified, and concentrated by microreversed phase chromatography, then analyzed by reversed-phase microcapillary liquid chromatography tandem mass spectrometry (LC/MS/MS) using both linear ion trap and hybrid linear ion trap–orbitrap mass spectrometers (*19*). We searched fragmentation spectra from data-dependent acquisitions against the reversed Swiss-Prot protein database using Sequest (*20*) and Mascot (*21*) algorithms. We identified eight total collagen peptide sequences, six from collagen α1 type I and two from collagen α2 type I. The eight peptides totaled 149 amino acids from four different samples (six LC/MS/MS data sets), nearly double the number of amino acids (89) recovered from *T. rex* (MOR 1125) (*4*, *5*). The eight peptides identified as collagen (Table 1) were top-ranked matches versus the Swiss-Prot target protein database. Four of the eight peptides, derived from three separate bone extracts, were sequenced from multiple scan events across multiple data files. We validated the sequences using scoring statistics, decoy databases, manual inspection, and spectral comparisons to high-confidence spectra obtained from synthetic peptides and peptides of identical sequence from extant organisms. One peptide sequence showed evidence of deamidation of asparagine, and all reported sequences contained at least one Pro-OH residue.

The eight peptide sequences for collagen α1 type I and collagen α2 type I represent 7.8 and 2.5% of the full-length sequence for related organisms, respectively. In addition, three peptide sequences were confirmed in a separate laboratory (in the lab of W.S.L.) from two samples from a single bone extraction. Coextracted sediment and buffer controls were consistently negative for collagen peptidic material by all methods of analyses including mass spectrometry sequencing, although common contaminants including human keratins, ubiquitous in all labs, and some microbial peptides were sequenced from these bone extracts.

All eight sequences derived from *B. canadensis* extracts are high-confidence, and their spectra produced expectation values of <1 from Mascot searches. Four dinosaur spectra were high-confidence matches to existing protein databases, and statistical validation is sufficient for identification. The four lowest-scoring MS/MS spectra from *Brachylophosaurus* bone extracts, acquired with the use of collision-induced dissociation (CID) in the linear ion trap of an LTQ-Orbitrap XL mass spectrometer, are shown in Fig. 3, A to D. These MS/MS spectra were subjected to an extra level of validation with the MS Search 2.0 spectral comparison algorithm from the National Institute of Standards and Technology (NIST) against a database of >200,000 random peptide fragmentation spectra from various taxa (*22*, *23*), including high-confidence versions of MS/MS spectra from four collagen sequences by adding previously acquired ostrich or synthetic peptides to the NIST spectral database. These four sequences derived from *B. canadensis* were top matches to high-confidence versions of the same sequences by fragment ion mass/charge ratio (m/z) values and relative intensities of fragment ions, providing additional validation of the data. All sequence data from *Brachylophosaurus* and validating sources are available in the supporting online material (SOM). The complete raw data from all 27,791 spectra, as well as previously reported sequences from *T. rex*, are available from the PRIDE database (www.ebi.ac.uk/pride/). In addition, we have shown *B. canadensis* collagen sequences to be statistically significant, and false discovery rates for MOR 2598 sequence data have been calculated (*10*).

In a separate lab (that of L.C.C.), *B. canadensis* bone extracts showed positive reactivity by immunoblot to a mixture of collagen type I polyclonal antibodies at high molecular weights (~250 to 300 kD), whereas surrounding sediments showed negative reactivity (fig. S9). This supports the identification of collagen fragments in bone extracts and suggests modifications (for example, cross-linking) of collagen molecules (*2*). Although silver-stained material in gels (fig. S2) suggest concentrations within the low end of current mass spectrometry sensitivity thresholds (low nanogram), it is likely that most of the protein is present in unsequenceable form(s); that is, cross-linked and/or modified so as to make them incapable of resolution by current mass spectrometry technology and software. We hypothesize that processes contributing to preservation of these otherwise labile components make analyses difficult, but conversely, the low recovery and diagenetic alteration support an endogenous source, as these chemical modifications are not observed in modern proteins.

B. canadensis collagen sequences were aligned with collagen sequences from 21 extant taxa and two extinct organisms: *Mammut americanum* (MOR 605) and *T. rex* (MOR 1125) (see table S1 and SOM appendix) (*6*). The *Anolis carolinensis* amino acid sequence was inferred with the use of FGENESH+ (gene prediction on the basis of protein homology; www.softberry.com). Additional collagen α2(I) sequence data for five species were obtained from online public databases (table S1).

We used BayesPhylogenies (*24*) to infer phylogenetic relationships from collagen sequences with the Dayhoff amino acid substitution model (*6*). The resulting consensus tree of the posterior distribution (Fig. 4) was well resolved, as was a phylogeny inferred by maximum likelihood (fig. S11). Whereas the first molecular phylogeny containing a non-avian dinosaurian [*T. rex*, MOR 1125, (*6*)] resulted in a tree that misplaced *A. carolinensis* (*6*), additional sequence data from several extant species (fig. S11 and table S1) corrected this misplacement and improved clade support to 100% (number of times a clade was inferred in the posterior distribution of trees) for all groups except the *Gallus*/*Struthio* group (Aves), which had 36% support. Under a majority-rule criterion to building a consensus tree, Dinosauria (the group containing the two extinct dinosaurs and the two birds) collapsed into a three-way polytomy.

Removing *T. rex* from the phylogeny resulted in a three-way polytomy as well. The amount of missing data in *B. canadensis* and *T. rex* sequences relative to extant samples resulted in relatively low resolution within Dinosauria, but even so, the phylogenetic relationship of recovered *B. canadensis* sequences supports the species' placement within Archosauria, closer to birds than *Alligator*. However, on the basis of well-established morphological analyses (*25*), we predict that *T. rex* is more closely related to birds than it is to the ornithischian hadrosaur *B. canadensis*. Despite ambiguity within Dinosauria, obvious phylogenetic signal resides within recovered collagen sequences, supporting endogeneity (fig. S11) (*10*).

The hypothesis that endogenous proteins can persist across geological time, as first reported for *T. rex* (MOR 1125), was met with appropriate skepticism (*7*–*9*). However, the inclusion of additional sequence data from extant reptiles (*6*) and *B. canadensis* strengthens the hypothesis that the molecular signal is preserved at least to the Late Cretaceous.

The submicron differences in texture (Fig. 1 and fig. S1), elemental differentiation, sub-"cellular" inclusions in osteocytes and vessels, identification of the posttranslational Pro-OH modification not produced by microbes (*18*), differential binding of antibodies by both in situ and immunoblot studies, collagen protein sequences, and phylogenetic analyses do not support a microbial origin for either these microstructures or peptide fragments (*7*). Coupled with evidence for cross-linking and unusual chemical modifications, the congruence of evidence strongly supports an endogenous origin for this material. The most parsimonious explanation, thus far unfalsified, is that original molecules persist in some Cretaceous dinosaur fossils. Still unknown is the chemistry behind such preservation.

References and Notes

1. M. H. Schweitzer, J. L. Wittmeyer, J. R. Horner, J. K. Toporski, *Science* **307**, 1952 (2005).
2. M. H. Schweitzer, J. L. Wittmeyer, J. R. Horner, *Proc. R. Soc. London Ser. B Biol. Sci.* **274**, 183 (2007).

3. M. H. Schweitzer *et al.*, *Science* **316**, 277 (2007).
4. J. M. Asara, M. H. Schweitzer, L. M. Freimark, M. Phillips, L. C. Cantley, *Science* **316**, 280 (2007).
5. J. M. Asara *et al.*, *Science* **317**, 1324 (2007).
6. C. L. Organ *et al.*, *Science* **320**, 499 (2008).
7. T. G. Kaye, G. Gaugler, Z. Sawlowicz, *PLoS One* **3**, e2808 (2008).
8. M. Buckley *et al.*, *Science* **319**, 33c (2008).
9. P. A. Pevzner, S. Kim, J. Ng, *Science* **321**, 1040b (2008).
10. Materials and methods are available as supporting material on *Science* Online.
11. S. Weiner, H. D. Wagner, *Annu. Rev. Mater. Sci.* **28**, 271 (1998).
12. S. Weiner, W. Traub, H. D. Wagner, *J. Struct. Biol.* **126**, 241 (1999).
13. D. N. Menton, D. J. Simmons, S. L. Chang, B. Y. Orr, *Anat. Rec.* **209**, 29 (1984).
14. M. L. Knothe Tate, J. R. Adamson, A. E. Tami, T. W. Bauer, *Int. J. Biochem. Cell Biol.* **36**, 1 (2004).
15. G. A. Wagnieres, M. Willem, W. M. Star, B. C. Wilson, *Photochem. Photobiol.* **68**, 603 (1998).
16. R. P. Mecham, J. E. Heuser, in *Cell Biology of the Extracellular Matrix*, E. D. Hay, Ed. (Plenum, New York, 1991), pp. 79–109.
17. P. S. Ebert, D. J. Prockop, *Biochem. Biophys. Res. Commun.* **8**, 305 (1962).
18. M. Rasmussen, M. Jacobsson, L. Björck, *J. Biol. Chem.* **278**, 32313 (2003).
19. Q. Hu *et al.*, *J. Mass Spectrom.* **40**, 430 (2005).
20. J. K. Eng, A. L. McCormack, J. R. Yates III, *J. Am. Soc. Mass Spectrom.* **5**, 976 (1994).
21. D. N. Perkins, D. J. Pappin, D. M. Creasy, J. S. Cottrell, *Electrophoresis* **20**, 3551 (1999).
22. H. Lam *et al.*, *Proteomics* **7**, 655 (2007).
23. J. M. Asara, M. H. Schweitzer, L. C. Cantley, J. S. Cottrell, *Science* **321**, 1040c (2008).
24. M. Pagel, A. Meade, *Syst. Biol.* **53**, 571 (2004).
25. D. Pisani *et al.*, *Proc. R. Soc. London Ser. B Biol. Sci.* **269**, 915 (2002).

26. We thank B. Harmon, N. Peterson, and the MOR crew responsible for recovery of MOR 2598; N. Equall and S. Brumfield for microscopy assistance; G. Fisher (Physical Electronics) for PHI nanoTOF assistance; T. Cleland for assistance with gel analyses; X. Yang for help with mass spectrometry sample preparation; S. Stein and Y. Mirokhin for MS Search 2.0 software enhancements; J. Starkey and R. Mecham for antibodies; B. Anderson for Fourier transform infrared spectroscopy access; T. Collier for sample preparation; E. Leithold for access to equipment; J. C. Fountain for support; and the Montana Department of Natural Resources and Conservation for land access. C.L.O. thanks S. V. Edwards for postdoctoral support. We acknowledge funding from NSF [awards EAR 0722702 and EAR 0634136 (J.M.A.) and EAR 0548847 and EAR-0541744 (M.H.S.)]; the David and Lucile Packard Foundation (M.H.S.); United Negro College Fund–Merck Postdoctoral Science Research Fellowship (M.B.D.); the Taplin Funds for Discovery (Harvard Medical School); partial support by NASA–Expermental Project to Simulate Competitive Research under grant NCC5-579 (R.A. and Z.S.); Damon Runyon Cancer Research Foundation (M.G.V.H.); NIH grants DK 55001, DK 62987, AA 13913, DK 61866, and CA 125550; and the Department of Medicine for the Division of Matrix Biology at the Beth Israel Deaconess Medical Center. Correspondence and requests for materials should be addressed to M.H.S. for biochemical and morphological analyses and to J.M.A. for mass spectrometry and molecular phylogenetics analyses.

Supporting Online Material

www.sciencemag.org/cgi/content/full/324/5927/626/DC1
Materials and Methods
SOM Text
Figs. S1 to S12
Table S1
References
Appendix S1
Database S1

25 August 2008; accepted 12 March 2009
10.1126/science.1165069

A Gross-Pitaevskii Treatment for Supersolid Helium

Philip W. Anderson

Understanding the observations of nonlinear rotational susceptibility in samples of solid helium below temperatures of 1 to 200 millikelvin (mK) has been a subject of some controversy. Here, the observations are conjectured to be describable in terms of a rarified Gross-Pitaevskii superfluid of vacancies, with a transition temperature of about 50 mK, whose density is locally enhanced by crystal imperfections. The observations can be greatly affected by this density enhancement. I argue that every pure Bose solid's ground state is a supersolid.

At least half a dozen groups by now have confirmed the original observation (*1*) made with a torsional oscillator that solid helium-4 (^{4}He) loses a fraction of its classical moment of inertia when it is below an onset temperature of around 200 mK. The first observations showed a strong dependence on velocity of motion; however, at lower temperatures, such as in the <50 mK range, the observations show thermal hysteresis, and in some circumstances the signal is quite robust. The observations can only indicate superfluid flow, though as yet no direct experiment has demonstrated that. However, an observed considerable sensitivity to crystal quality leaves open the question of whether the flow is intrinsic to the pure solid; a vocal faction argues that it cannot be. I here address these issues from a different point of view.

The Gross-Pitaevskii equation for the order parameter (*2*, *3*), and the corresponding free energy, has become standard for treating Bose condensation in cold atomic gases. The assumption on which this theory was based, essentially that the bosons are dilute relative to the range of their interaction, are well satisfied in these systems but not for superfluid helium (He II) (correspondingly, there are complications in He II, specifically the roton spectrum and the large depletion of the condensate). One might think that the Gross-Pitaevskii equation would be even less applicable to solid He, but the opposite may be the case.

The solid is of course dense, but the experiments indicating supersolidity show that the amount of matter that actually flows is a few percent of the atoms, and in good crystals much less matter flows than that. The earliest theoretical paper on supersolidity (*4*) proposed that supersolidity might consist of Bose condensation of a small density of vacancies in the solid substrate. The wave function that I have proposed as a heuristic description of the phenomena (*5*) can be interpreted in those terms. Vacancy flow within a rigid lattice and substrate atom flow are essentially equivalent, so as a shorthand I will discuss "vacancies" and a quantum (boson) field representing them. The term vacancies is used henceforth as a shorthand for the fluctuations in particle number that make it possible to define a phase of the particle field. In the pure crystal, they may be equally matched between particles and holes, and the superfluidity can be caused by an overlap of local boson wave functions [see the supporting online material (SOM) text].

Vacancies certainly interact repulsively as hard-core bosons, because no two vacancies can be on the same site. There may also be a long-range interaction due to elasticity, which is thought to be attractive but probably does not play any dynamical role; elasticity simply changes the chemical potential. The vacancy density is, especially in a good crystal, very low and experimentally on the order of 3×10^{-4} per site.

The Gross-Pitaevskii energy is

$$E = |(\hbar\nabla\Psi)|^2/2m^* + V(r)|\Psi|^2 + \frac{1}{2}g|\Psi|^4 \quad (1)$$

and the Gross-Pitaevskii equation is

$$\mu\Psi = -\hbar^2\nabla^2\Psi/2m^* + V(r)\Psi + g|\Psi|^2\Psi \quad (2)$$

Here, $\hbar$ is the reduced Planck constant, Ψ is the "order parameter" (the mean of the vacancy boson field), m^* is an effective mass, g is the coupling constant ($\hbar^2 a/\pi m^*$, where a is the scattering length and presumed repulsive), and μ is the chemical potential for vacancies. $V(r)$ is in the gas state simply the trap potential, but in here $V(r)$ is included to take into account the fact that dislocations, surfaces, grain boundaries, and possibly ^{3}He impurities are all attractive sites for vacancies. All of these parameters and their values need further discussion because my physical conclusions depend on them. Equation 1 essentially is just a coarse-graining of the mean-field Schrödinger equation. The time-dependent equation that controls collective modes and vortex behavior is obtained by replacing μ with $\frac{\hbar\partial}{i\partial t}$.

The chemical potential tells us how many vacancies there are. The strong arguments presented in (*6*, *7*), which are based on a Bijl-Jastrow wave

Department of Physics, Princeton University, Princeton, NJ 08525, USA.